Interplay between excitability type and distributions of neuronal connectivity determines neuronal network synchronization

Sima Mofakham, Christian G. Fink, Victoria Booth, and Michal R. Zochowski

Phys. Rev. E **94**, 042427 — Published 31 October 2016

DOI: 10.1103/PhysRevE.94.042427

Interplay between excitability type and distributions of neuronal connectivity determines neuronal network synchronization

Sima Mofakham[1], Christian G. Fink[2], Victoria Booth[3], Michal R. Zochowski[4]

[1]Biophysics Program, University of Michigan,

[2] Physics Dept. and Neuroscience Program, Ohio Wesleyan University,

[3] Mathematics Dept. and Anesthesiology Dept., University of Michigan,

[4] Department of Physics and Biophysics Program, University of Michigan

Abstract

While the interplay between neuronal excitability properties and global properties of network topology is known to affect network propensity for synchronization, it is not clear how detailed characteristics of these properties affect spatio-temporal pattern formation. Here, we study mixed networks, composed of neurons having Type I and/or Type II phase response curves, with varying distributions of local and random connections and show that not only average network properties, but also the connectivity distribution statistics, significantly affect network synchrony. Namely, we study networks with fixed network-wide properties, but vary the number of random connections that nodes project. We show that varying node excitability (Type I vs Type II) influences network synchrony most dramatically for systems with long-tailed distributions of the number of random connections per node. This indicates that a cluster of even a few highly re-wired cells with a high propensity for synchronization can alter the degree of synchrony in the network as a whole. We show this effect generally on a network of coupled Kuramoto oscillators and investigate the impact of this effect more thoroughly in pulse coupled networks of biophysical neurons.

Key words: synchronization, neuronal excitability, phase response curve, and network architecture

I. Introduction

Synchronization in complex networks has been studied extensively over the last two decades [1],[2],[3],[4],[5]. In the brain, synchronization of neuronal populations has been associated with many brain functions, including attention and memory formation [6],[7],[8],[9]. On the other hand, aberrant synchrony is implicated in many pathologies of the brain, such as epilepsy [10], Parkinson's disease [11],[12], and schizophrenia [13], underscoring the need to better understand mechanisms that generate and promote synchronization of neuronal networks.

Generally, the emergence of synchronous spatiotemporal activity patterns may be explained by two broad classes of mechanisms: 1) excitability properties of individual network nodes, and 2) characteristics of network coupling statistics. Neuronal excitability falls into one of two categories, depending on the bifurcation structure observed in the neuron's transition to firing. In Type I neurons, repetitive spiking is initiated by a saddle-node on an invariant cycle (SNIC) bifurcation. These neurons act as integrators, with firing frequency increasing sharply from the arbitrarily low levels observed at firing threshold, and they exhibit a low propensity for synchrony when coupled by excitation. Type II neurons transition to firing through an Andronov-Hopf bifurcation, leading to a discontinuous and shallow frequency-current curve, and higher propensity for synchronization when coupled together [14],[15],[16],[17]. Generally, these excitability types result in different profiles of the neuronal phase response curve (PRC), which captures the neuronal response to brief stimulation [18],[19],[20]. Usually, Type I cells exhibit exclusively phase advances in response to excitatory stimuli arriving at different times during the firing cycle, while Type II cells display both phase delays and advances. Experimental results show that both of these cell types are present in the brain, with some neurons capable of switching types [21].

Different frameworks for network connectivity have been used to investigate the influence of network topology upon neuronal synchronization [22]. Among these frameworks, small-world and scale free architectures have been widely used. The small-

world regime is defined as having a high clustering coefficient and small path length [23],[24],[25],[26] . The Watts-Strogatz model uses a single parameter, the rewiring probability, to transition between a locally connected network, through the small world regime to a completely random network [27]. The scale free architecture introduces highly interconnected neurons called hub cells, which have been shown to orchestrate synchrony in experimental models of epilepsy [28],[29],[30]. A derivative of the latter is the "rich club" structure [31],[32],[33],[34],[35] in which hub cells are interconnected amongst themselves. We have shown in previous work that feedback between neuronal excitability type and network structure dramatically influence network synchrony [36]. Namely, we showed that Type II networks synchronize to much higher degree than their identical Type I counterparts. Recently we have also shown that in scale-free networks with mixed Type I and Type II cells, synchronization is enhanced by placing Type II cells (rather than Type I cells) as hubs [37].

In the case of small world connectivity, the network properties are assessed globally for the whole system, whether through estimation of mean path length and clustering coefficient or rewiring probability. Here we introduce a Watts-Strogatz type of small-world model having heterogeneous structure in which each cell is assigned an individual rewiring probability. We vary distribution statistics (i.e. we use exponential, Poisson and uniform distributions) of these rewiring probabilities but constrain the average, network-wide rewiring probability to be constant (Fig 1). We then compare the effect of interactions between placement of node excitability type and statistics of network connectivity structure. Namely we compare the case in which highly re-wired (HWR) nodes have Type I excitability with the opposite case, in which highly re-wired nodes are Type II. We perform this comparison in a system of continuously coupled Kuramoto oscillators [38], [39],[40] and in networks of pulse coupled biophysical model neurons. Our results show that, generally, networks in which Type II cells have a large number of re-wired connections synchronize much better than those in which Type I cells are highly re-wired. However, the degree of synchronization depends on the distribution of re-wired connections per cell. Specifically, we show that distributions with a relatively longer tail of re-wired connections per cell, such as an exponential distribution in our case, can

increase the propensity for network synchronization, depending on excitability type, indicating that a few highly re-wired cells may drive synchrony in a network as a whole. Finally, we investigate the effect of forming clusters among the highly re-wired cells, or "rich clubs," and show that interconnecting the most highly re-wired cells enhances synchronous dynamics when such cells are Type II, but not when they are Type I. These results indicate that the distribution of structural heterogeneities within the network is an important factor in spatio-temporal pattern formation and that relatively few preferentially connected nodes can drive network wide synchrony.

II. Continuously coupled Kuramoto oscillators

We first investigate the impact of connectivity distributions and excitability type on spatio-temporal pattern formation in a system of continuously coupled Kuramoto oscillators. Here, the phase dynamics were governed by:

$$\frac{d\phi_i}{dt} = \omega_i + A\sum_{j=1}^{N} G\left(r_{i,j}\right)K\left(\phi_i,\phi_j\right), \quad (1)$$

where, ω_i is the natural frequency of the i-th oscillator, G is the connectivity matrix and and K denotes the phase coupling function. We modified the phase coupling to be able to continuously change the phase response curve:

$$K\left(\phi_i,\phi_j\right) = u\left(\sin\left(\phi_i-\phi_j\right)\right)-\left(1-u\right)\left(\sin\left(\frac{\left(\phi_i-\phi_j\right)}{2}\right)\right) \quad (2)$$

Depending on the parmeter *u* oscillators continuously transition from Type I to Type II PRC.

The networks were composed of 1000 oscillators with 4% connectivity (40 outgoing connections per node), situated in a one-dimensional ring with periodic boundary conditions.

In the standard Watts–Strogatz small-world connectivity paradigm, each synaptic connection is assigned the same re-wiring probability, which determines whether its target will remain a neighboring cell or be re-wired to a random target cell in the network (independent of their distance). This paradigm results in an approximately Poisson distribution for the number of re-wired outgoing connections per neuron (Fig. 1 top-row). Here, we modified the standard Watts–Strogatz's connectivity (where every connection in the network is re-wired with predefined probability) by first specifying the global re-wiring fraction within the network (P), and consequently the total number of re-wired connections. We then employed a specified distribution to assign the number of re-wired connections projecting from each individual neurons. We used three different distributions: a) "No Variance" distribution, in which all neurons shared the same number of re-wired connections, b) Uniform distribution with a defined average and fixed variance (Fig. 1 middle-row), and c) Exponential distribution (Fig. 1 bottom-row). We then compare these connectivity paradigms with conventional small-world topology, which has a Poisson distribution of re-wired connections per cell.

We defined two, equally sized populations of nodes having a Type I PRC (u = 0.0) or a Type II PRC (u=1.0), (Fig. 2a) and subsequently studied network spatio-temporal patterning for two cases: 1) when Type I oscillators had highly re-wired connections and, 2) when Type II oscillators were highly re-wired. We measured the change in synchrony for varying coupling strength A.

We measured synchrony using the so-called synchrony index defined in [30-31]. The measure is based on the calculation of the mean population-averaged fluctuations over an extended period of time, normalized to the average of individual neurons' fluctuations. In order to calculate the synchrony index (λ) from spike timings, they were convolved with a Gaussian (here we used a 2ms width; the obtained results are not dependent on the Gaussian width), averaged across all neurons at each time point, and the variance across time was computed ($\sigma_V^2 = \left\langle [V(t)]^2 \right\rangle_t - [\left\langle V(t) \right\rangle_t]^2$). The variances of individual neuronal voltage traces across time were computed, and then averaged over all neurons ($\sigma_{V_i}^2$). Namely, λ was then computed as:

$$\lambda = \sqrt{\frac{\sigma_V^2}{\frac{1}{N}\sum_{i=1}^{N}\sigma_{V_i}^2}} \quad (6)$$

λ is bounded between 0 and 1, zero for asynchronous dynamics and 1 for complete synchrony across the network.

We generally observed a change in degree of synchrony when Type II nodes were highly re-wired, with overall synchrony increasing with coupling strength (Fig. 2b). However by far the largest change in the degree of synchrony was observed when the rewiring probabilities were drawn from an exponential distribution (Fig. 2b, black/light gray dashed line).

III. Network of pulse coupled neurons.

We next investigate the impact of this result in networks of pulse coupled biophysical model neurons. We employed a Hodgkin Huxley type neuronal model with a fast inward Na^+ current, delayed rectifier K^+ current, and a leakage current. Cholinergic modulation has been experimentally shown to switch the PRCs of cortical neurons from Type II to Type I [21]. This effect is known to be driven by a slow, M-type K^+ current (gated by g_{Ks}) responsible for spike frequency adaptation [29]. The equation governing neuronal dynamics is given by:

$$C\frac{dV_i}{dt} = -g_{Na}m_\infty^3(V_i)h(V_i - V_{Na}) - g_{Kdr}n^4(V_i - V_K) - g_{Ks}S(V_i - V_K) - g_L(V_i - V_L) + I^{drive} + I_{ij}^{syn} \quad (3)$$

where C =1.0 μ F/cm^2 and I_{ij}^{syn} is the synaptic current. The synaptic current from neuron 'j' to 'i' is governed by:

$$I_{ij}^{syn} = W\exp(-\frac{t - t_j}{\tau})(E_{syn} - V_i) \quad (4)$$

where t_j is the spike time of neuron j, and W is the synaptic strength which was kept

constant for all the connections, and we fixed τ =0.5 ms and E_{syn}=0 mV. I^{drive} is an externally applied current that remains constant for each neuron within a simulation, but depending on the heterogeneity level needed for each simulation the spread of external current across neurons was set appropriately. In all the simulations in this paper, except Fig. 7, the I^{drive} was set to generate an average of 15 Hz with frequency spread of 26.6%, Type I: $I^{drive} = 0.158 \pm 0.038$, Type II: $I^{drive} = 1.22 \pm 0.18$. For the results presented in Fig. 7 the frequency spread changes from 0% (0Hz) to 52% (8Hz), Type I: $I^{drive} = 0.158 \pm 0.076$; Type II: $I^{drive} = 1.22 \pm 0.37$. The value of constant parameters used in this model are the same for both Type I and Type II neurons except g_{Ks} which is g_{Ks}=0.1 mS/cm^2 for Type I and g_{Ks}=0.8 mS/cm^2 for Type II neurons: g_{Na} = 24.0 mS/cm^2, g_{Kdr} = 3.0 mS/cm^2, g_L = 0.02 mS/cm^2, V_{Na} = 55.0 mV, V_K = –90.0 mV, and V_L = –60.0 mV.

In equation (3) m_∞ and h are responsible for activation and inactivation of the Na current, and their dynamics are governed by $m_\infty(V) = 1/(1 + e^{(-V - 30.0)/9.5})$ and $dh/dt = \alpha_h(h_\infty(V) - h)/\tau_h(V)$, with $h_\infty(V) = 1/(1 + e^{(V + 53.0)/7.0})$ and $\tau_h(V) = 0.37 + 2.78/(1 + e^{(V + 40.5)/6.0})$. The dynamics of the gating variable for the delayed rectifier potassium current were given by $dn/dt = (n_\infty(V) - h)/\tau_n(V)$, with $n_\infty(V) = 1/(1 + e^{(-V - 30.0)/10.0})$ and $\tau_n(V) = 0.37 + 1.85/(1 + e^{(V + 27.0)/15.0})$. Finally, the gating variable for the slow, M-type potassium current was governed by $ds/dt = \alpha_s (s_\infty(V) - s)/75.0$, and $s_\infty(V) = 1/(1 + e^{(-V - 39.0)/5.0})$. The parameter values were adopted from [21] and are established experimentally.

We model the acetylcholine mediated change in the PRC by decreasing g_{Ks} from 0.8 mS/cm^2 to 0.1 mS/cm^2. This mimics the effect of acetylcholine in switching the neuronal PRC from Type II to Type I [43]. Figure 3a depicts the PRC for these two cases, calculated using the following equation:

$$\Delta(\theta) = \frac{T_{Original} - T_{Perturbed}(\theta)}{T_{Original}} \tag{5}$$

where θ is the phase at which the input is received, $T_{original}$ is the period of the unperturbed oscillator, $T_{perturbed}$ is the duration of the spike cycle during which the input is received, and Δ can be positive (phase advance) or negative (phase delay).

We considered networks composed of 1000 excitatory cortical pyramidal cells with the same connectivity as in the coupled Kuramoto system described above. For the majority of our results, we set the total number of re-wired connections, or global re-wiring fraction P, to 15% (which essentially corresponds to a re-wiring probability of $p = 0.15$ in the standard Watts-Strogatz connectivity paradigm). As before, we constructed networks of excitatory cells with mixed 50% - 50% Type I and Type II excitability properties.

As in the case of the Kuramoto network, to investigate the interplay between the statistics of network structure and cellular excitability in generating network dynamics, we compare two different regimes: (a) Type I Highly Re-wired (HRW), in which neurons with higher numbers of re-wired connections are selectively assigned Type I excitability and those with lower numbers of re-wired connections assigned Type II excitability (Fig. 1b, left column), and (b) Type II HRW, in which neurons with higher numbers of re-wired connections are selectively assigned Type II excitability and those with fewer re-wired connections are Type I (Fig. 1b, right column).

We first compared (Fig 3c) network synchrony (using synchrony index as above) for each connectivity distribution for the two cases of Type I HRW (light gray curves) and Type II HRW (black curves), as a function of synaptic strength W. For all connectivity architectures, the Type II HRW networks exhibited significantly higher synchrony in comparison with the Type I HRW networks. However, the largest difference in synchrony for Type II HRW versus Type I HRW regimes occurred for the exponential distribution, which has the widest range of ratios of re-wired to local connections across cells. In this regime, the excitability type of the few neurons that have all or most of their connections re-wired resulted in dramatically different network dynamics. As shown in the raster plots of Fig. 3d (first and second columns), network synchrony is visibly increased when the highly re-wired cells have Type II excitability. Further, increases in

the synaptic strength W drove both Type I HRW and Type II HRW networks out of synchrony (Fig. 3d, third column). This was primarily due to the mismatch of Type I and Type II firing responses to increased excitation, dictated by their disparate F-I curves, as well as a transition to bursting.

To check whether the observed increase in synchrony was solely due to higher synchronization only among the Type II cells, we separately measured the synchrony index in each population for the two cases (Fig. 4a,b). The increase of synchrony was more pronounced for the Type II neurons when they were highly re-wired (Fig 4b) but was also observed for the Type I neurons for the same case (Fig 4a). This indicates that Type II neurons can lead both populations of neurons to synchronous activity, whereas if Type I neurons have more long-distance connections, they attenuate the emergence of synchronous spatio-temporal patterns.

In contrast to these mixed cell networks, the dynamics of homogeneous networks composed solely of either Type I or Type II neurons (Fig. 5) are much less sensitive to variations in network connectivity architecture. Figure 5a displays the synchrony index for homogeneous networks of Type I and Type II neurons as a function of synaptic weight W for Poisson, uniform, exponential and no variance re-wiring distributions. The homogeneous Type I networks show no signs of synchrony for any of the connectivity paradigms (light gray line along bottom axis). On the other hand, Type II networks show a significant tendency to synchronize, and increasing coupling strength leads to highly synchronous dynamics in all connectivity frameworks. Again, an extreme increase in the synaptic weight drives the network dynamics out of synchrony, in agreement with previous results showing that increasing the firing rate of Type II neurons leads to the disappearance of the phase delay region of the PRC, adversely affecting network synchrony [37].

These divergent effects on network synchrony are due to the interplay between individual neuronal properties and network architecture, and were robust for low values of global re-wiring fraction P and for different fractions of cell types in the network. As illustrated in Figure 6a, the difference between Type I HRW and Type II HRW scenarios (inset) was greatest for small values of global rewiring fraction, namely P = 0.1 - 0.2, which corresponds to the small-world network regime. As P increased further, synchrony increased overall, and the differences across connectivity distributions decreased, due to the introduction of many re-wired connections. When the fraction of Type II cells in the network was varied from 50% (Fig 6b), differences in network synchronization remained between the Type I and Type II HRW scenarios, with the greatest differences occurring when less than half of the cells were Type II (inset).

We also examined the influence of heterogeneity in intrinsic cellular firing frequency on the difference in network synchrony between the Type II HRW and Type I HRW scenarios (Fig. 7). While the mean neuronal firing frequency remained 15 Hz, we varied its spread around that value. When heterogeneity was low, networks tended to synchronize regardless of their connectivity structure, but by increasing the heterogeneity, Type II HRW networks maintained synchronization, while it quickly degraded in Type I HRW networks. The greatest difference between scenarios occurred for a range of 12-18 Hz (spread of 40%) in intrinsic cellular frequencies for networks with the exponential and Poisson re-wiring distributions, as shown in the raster plots in Figure 7b. For larger heterogeneity in firing frequencies, networks in either the Type I or Type II HRW scenarios were not able to synchronize.

IV. Synchrony in networks with high connectivity clusters

We also investigated effects on network synchrony when clusters among either highly re-wired Type I cells or highly re-wired Type II cells were formed (Fig. 8). We created clusters among the top fractions of highly re-wired neurons by interconnecting all neurons within that group. Here we set the synaptic strength to be such that both types of

networks, Type I HRW and Type II HRW, did not show significant synchrony (W=0.005 mS/cm^2, Fig. 8b panels I and II). We then added connections between different fractions of the most highly re-wired neurons. In Type I HRW networks, interconnecting up to 12% of the most highly re-wired cells did not appreciably change the degree of synchrony in the system (Fig. 8a, light gray curves, Fig. 8b panel III). In Type II HRW networks, however, even a small fraction of additional connections among the most re-wired cells increased network synchronization (Fig. 8a black curves, Fig. 8b panel IV). Thus, these results indicate that a cluster consisting of a few Type II neurons with long-distance connections can drive network dynamics toward synchrony, while a similar connectivity structure involving Type I neurons does not facilitate the emergence of synchronous activity. To explore whether the emergence of synchrony was due to interconnecting Type II neurons, regardless of their connectivity, or whether their long-range connections made a difference, we performed simulations in which we formed clusters among Type II or Type I neurons with the lowest number of re-wired connections (Fig. 8a green and purple curves, respectively). Synchronization increased with the formation of clusters among Type II cells in the uniform distribution networks and particularly in the exponential distribution networks, but higher synchronization was exhibited when the clustered cells were highly re-wired. In particular, in the exponential distribution networks, forming a cluster of minimally re-wired Type II neurons resulted in the formation of domains of local synchronous activity (Fig. 8b panel V), but the overall level of synchrony was lower as compared to the case when the most highly re-wired Type II neurons formed a cluster (Fig. 8b panel IV). Interconnecting minimally re-wired Type I neurons in a cluster did not affect synchrony (Fig. 8a purple curves), as expected from the lack of effect of clusters of highly re-wired Type I neurons. These results show that the excitability type of the neurons within a cluster as well as the statistics of their connectivity play an important role in facilitating the emergence of global synchrony.

VII. Discussion

In this study we have explored the interaction between excitability properties and local connectivity characteristics of individual nodes in affecting network synchronization. Namely, we investigated how the effects of structural network heterogeneities coupled with varying nodal dynamics can lead to modifications in network-wide activity patterns. We studied this phenomenon for a system of continuously coupled Kuramoto oscillators and investigated its impact in networks of pulse coupled biophysical model neurons. For Kuramoto oscillators, we modified the phase coupling to model a continuous switch from Type I to Type II coupling responses. In the neuronal networks, we varied activation of the muscarinic receptor which is known to mediate the transition between Type I and Type II PRCs. The results are largely the same for both systems. The nodes in the network were allowed to have varying numbers of re-wired connections, while at the same time their excitability exhibited Type I or Type II characteristics. We varied the network distributions of re-wired connections per node between Poisson, uniform and exponential distributions. We showed that highly re-wired nodes of Type II excitability facilitate increased levels of network-wide synchrony. They form a distributed backbone in the network driving other nodes toward synchrony. This effect was exacerbated in the re-wiring distribution having the longest tail (namely the exponential distribution). This distribution exhibited the greatest change in synchrony when the excitability type of the nodes with the highest numbers of re-wired connections was changed from Type I to Type II. This indicates that relatively few highly re-wired Type II cells can significantly increase the level of network-wide synchrony. However, increased synchronization is not realized when these highly re-wired nodes have Type I excitability.

In the neuronal networks, the effect of a small population of highly-re-wired Type II cells on synchrony was further exacerbated when we allowed these highly re-wired Type II cells to form connected clusters. In this case even a small Type II cluster, irrespective of whether it was formed from highly re-wired cells or minimally re-wired cells, drove a significant increase in network-wide synchrony. For exponential distribution networks, the difference in improved synchronization induced by clusters of highly re-wired compared to minimally re-wired Type II cells was greatest, reflecting the large

differential in the number of re-wired connections per cell at either end of the distribution.

Thus, our results indicate that heterogeneity in cellular connectivity, and subsequently not only the first moment but also the second moment of connectivity statistics, are important for spatio-temporal pattern formation in the network. This result may have significant implications for characterizing real-world network connectivity patterns, since often connectivity statistics are known only for a few identified cells. We show that relatively few cells of specific dynamical and connectivity properties can significantly change spatio-temporal patterning.

We note that our neuronal networks were limited only to excitatory cells. We have previously shown, however, that general differences between Type I and Type II network synchronizability remains unchanged with the addition of inhibitory cells to the network [36]. The one-dimensional topology on which we base our networks is also clearly unrealistic, but again the general synchrony results are known to hold for higher dimensional systems. Furthermore, the addition of connection shortcuts makes the notion of initial dimensionality largely irrelevant.

The results of this study may be pertinent for the modulation of neuronal excitability in the brain during sleep and wake states. It has been shown that the intrinsic excitability of neurons can be modulated by acetylcholine levels [21]: high levels of acetylcholine (ACh), during waking and rapid eye movement (REM) sleep, drive neuronal excitability towards Type I behavior, while the absence of ACh during slow wave sleep pushes excitability towards Type II. We show that relatively few neurons expressing receptors that are sensitive to ACh levels can dramatically change network-wide dynamics.

The synchronizing role of the Type II clusters maybe also be important to understanding pathological brain activity. It has been shown that upon an injury to the dentate gyrus, its circuits undergo architectural rearrangements, which include formation of recurrent connections among excitatory granule cells. These changes make its circuit hyper-excitable and prone to generating epileptic seizures [44],[45],[46]. Morgan and Soltesz showed that even by keeping the number of connections constant throughout the network

while assigning more connections to a few granule cells and interconnecting these hubs can create a circuit with hyper-excitable characteristics prone to generating seizure like activity [47]. Our results suggest that seizure promotion by this mechanism would be strengthened if the interconnected cells had Type II excitability properties.

Acknowledgements: This work was supported in part by NIH NIBIB EB018297 (MZ, VB), NSF PoLS 1058034 (MZ) and NSF DMS-1412119 (VB).

References:

[1] Y. Eom, S. Boccaletti, G. Caldarelli, Nat. Publ. Gr. 1 (2016).
[2] S. Assenza, R. Gutie, V. Latora, S. Boccaletti, 1 (2011).
[3] S. Yu, D. Huang, W. Singer, D. Nikolic, 2891 (2008).
[4] P.J. Uhlhaas, W. Singer, Neuron **52**, 155 (2006).
[5] A. Arenas, D. Albert, Phys. Rep. **469**, 93 (2008).
[6] P.N. Steinmetz, a Roy, P.J. Fitzgerald, S.S. Hsiao, K.O. Johnson, E. Niebur, Nature **404**, 187 (2000).
[7] P. Fries, J.H. Reynolds, a E. Rorie, R. Desimone, Science **291**, 1560 (2001).
[8] J. Fell, P. Klaver, K. Lehnertz, T. Grunwald, C. Schaller, C.E. Elger, G. Fernández, Nat. Neurosci. **4**, 1259 (2001).
[9] U. Rutishauser, I.B. Ross, A.N. Mamelak, E.M. Schuman, Nature **464**, 903 (2010).
[10] P. Jiruska, M. de Curtis, J.G.R. Jefferys, C.A. Schevon, S.J. Schiff, K. Schindler, J. Physiol. **591**, 787 (2013).
[11] J.A. Goldberg, U. Rokni, T. Boraud, E. Vaadia, H. Bergman, J Neurosci **24**, 6003 (2004).
[12] T. Wichmann, M.R. Delong, J. Guridi, J. a. Obeso, Mov. Disord. **26**, 1032 (2011).
[13] P.J. Uhlhaas, W. Singer, Nat. Rev. Neurosci. **11**, 100 (2010).
[14] E.M. Izhikevich, Dynamical Systems in Neuroscience, 2007.
[15] C.G. Fink, V. Booth, M. Zochowski, PLoS Comput. Biol. **7**, 1 (2011).
[16] S. Marella, G.B. Ermentrout, Phys. Rev. E - Stat. Nonlinear, Soft Matter Phys. **77**, 1 (2008).
[17] S. Achuthan, C.C. Canavier, J. Neurosci. **29**, 5218 (2009).
[18] G.B. Ermentrout, Neural Comput. **8**, 979 (1996).
[19] J. Rinzel, G.B. Ermentrout, in:, Methods Neuronal Model., 1989, pp. 251–292.
[20] B.S. Gutkin, G.B. Ermentrout, A.D. Reyes, J. Neurophysiol. **94**, 1623 (2005).
[21] K.M. Stiefel, B.S. Gutkin, T.J. Sejnowski, PLoS One **3**, e3947 (2008).
[22] S. Boccaletti, V. Latora, Y. Moreno, M. Chavez, D.-U. Hwang, Phys. Rep. **424**, 175 (2006).
[23] D.J. Watts, S.H. Strogatz, Nature **393**, 440 (1998).
[24] C. Li, G. Chen, Phys. Rev. E, **68**, 2 (2003).

[25] W.J. Yuan, X.S Luo, R.H. Yang, Chinese Physics Letters, **24**, 3 (2007).

[27] D.J. Watts, S.H. Strogatz, Nature **393**, 440 (1998).

[28] A.-L. Barabási, R. Albert, Science (80-.). **286**, 509 (1999).

[29] P. Bonifazi, M. Goldin, M.A. Picardo, I. Jorquera, A. Cattani, G. Bianconi, a Represa, Y. Ben-Ari, R. Cossart, Science (80-.). **326**, 1419 (2009).
[30] J.M. Beggs, D. Plenz, J. Neurosci. **23**, 11167 (2003).
[31] M.P. van den Heuvel, O. Sporns, J. Neurosci. **31**, 15775 (2011).
[32] N. a Crossley, A. Mechelli, P.E. Vértes, T.T. Winton-Brown, A.X. Patel, C.E. Ginestet, P. McGuire, E.T. Bullmore, Proc. Natl. Acad. Sci. U. S. A. **110**, 11583 (2013).
[33] M. a de Reus, M.P. van den Heuvel, J. Neurosci. **33**, 12929 (2013).
[34] E.K. Towlson, P.E. Vértes, S.E. Ahnert, W.R. Schafer, E.T. Bullmore, J. Neurosci. **33**, 6380 (2013).
[35] M.P. van den Heuvel, R.S. Kahn, J. Goñi, O. Sporns, Proc. Natl. Acad. Sci. U. S. A. **109**, 11372 (2012).
[36] A. Bogaard, J. Parent, M. Zochowski, V. Booth, J. Neurosci. **29**, 1677 (2009).
[37] M.J. Leone, B.N. Schurter, B. Letson, V. Booth, M. Zochowski, C.G. Fink, Phys. Rev. E **91**, 1 (2015).
[38] Y. Kuramoto. Chemical Oscillations, Waves, and Turbulence. Berlin: Springer-Verlag (1984).
[39] J.A. Acebr, V. Gradenigo, D. Matematica, Rev. Mod. Phys. **77**, 1 (2005).
[40] S.H. Strogatz, Phys. D Nonlinear Phenom. **143**, 1 (2000).
[41] K.M. Stiefel, B.S. Gutkin, T.J. Sejnowski, J. Comput. Neurosci. **26**, 289 (2009).
[42] D. Golomb, J. Rinzel, Phys. Rev. E **48**, 4810 (1993).
[43] D. Golomb, J. Rinzel, Phys. D Nonlinear Phenom. **72**, 259 (1994).
[44] J. Dyhrfjeld-Johnsen, V. Santhakumar, R.J. Morgan, R. Huerta, L. Tsimring, I. Soltesz, J. Neurophysiol. **97**, 1566 (2007).
[45] P.S. Buckmaster, a L. Jongen-Rêlo, J. Neurosci. **19**, 9519 (1999).
[46] V. Santhakumar, I. Aradi, I. Soltesz, J. Neurophysiol. **93**, 437 (2005).
[47] R.J. Morgan, I. Soltesz, Proc. Natl. Acad. Sci. **105**, 6179 (2008).

FIGURE CAPTIONS

Figure 1. a) Examples of connectivity matrices for three different distributions of rewiring probability of individual cells b) Histograms of the number of neurons with a specific number of re-wired connections for the standard Poisson (top row), uniform (middle row) and exponential (bottom row) re-wiring distributions for Type I (left column) and Type II Highly Re-wired scenarios (right column), for a mixed network of 50% Type I and 50% Type II cells. In the Type I Highly Re-wired scenario (left column panels), neurons with the higher number of re-wired outgoing connections have Type I excitability characteristics (light gray bars), while in the Type II Highly re-wired scenario (right column panels) Type II neurons have a higher number of re-wired outgoing connections (black bars).

Figure 2. Synchrony in a heterogeneous network of Type I and Type II coupled Kuramoto oscillators (N=1000). a) Corresponding PRC for different values of the parameter *u* that switches the synchronization properties of the Kuramoto oscillators b) Synchrony index as a function of coupling strength for various distributions of rewiring probability of nodal connections: no variance (dark gray solid line), uniform (solid lines), Poisson (dotted lines) and exponential (dashed lines). Type I Highly Re-wired (Type I HRW) nodes are denoted in light gray; Type II HRW in black. Averaged network wide rewiring probability is p=0.15.

Figure 3. Network of pulse coupled neurons. a,b) Phase response curves (PRCs) and frequency-current (F-I) curves for Type I (g_{Ks}=0.1 mS/cm^2 , light gray curves) and Type II (g_{Ks}=0.8 mS/cm^2, black curves) neurons. c) Synchrony in a heterogeneous network of Type I (50%) and Type II (50%) neurons as a function of synaptic strength for no variance (dark gray solid line), uniform (solid lines), Poisson (dotted lines) and exponential (dashed lines) distributions for the Type I Highly Re-wired (Type I HRW, light gray curves) and Type II Highly Re-wired (Type II HRW, black curves) scenarios. The networks in these simulations have a global re-wiring fraction of P=0.15 and cellular frequency distribution of 15±2 Hz. d) Examples of raster plots (light gray dots: Type I neurons, black dots: Type II neurons) for exponential distribution networks with synaptic strengths of W=0.0075 (left column), 0.01 (middle) and 0.02 mS/cm^2 (right column) in the Type I HRW (top row) and Type II HRW (bottom row) scenarios.

Figure 4. Synchronization characteristics of Type I and Type II subpopulations. a) Synchrony in a heterogeneous network of Type I (50%) and Type II (50%) neurons within Type I cell group; b) synchrony within Type II cells as a function of synaptic weight. Synchrony increases within both populations when the Type II population is highly re-wired, indicating that Type II cells mediate synchrony within the whole network. The networks in these simulations have a global re-wiring fraction of P=0.15 and cellular frequency distribution of 15±2 Hz.

Figure 5. Synchrony in homogeneous networks of Type I and II neurons as a function of synaptic weight. (a) Type I networks display highly asynchronous dynamics for all connectivity paradigms and for synaptic weights as high as W=0.02 mS/cm^2. Homogeneous networks of Type II neurons, however, readily synchronize for small and intermediate synaptic strengths. (b) Raster plots of network activity for Type I (top row) and Type II (bottom row) networks with synaptic strengths

of W=0.0075 mS/cm^2 (left column) and W=0.02 mS/cm^2 (right column). Note different time scales. Here the exponential connectivity paradigm was employed, with the same parameters for Type I and Type II simulations (P=0.15, intrinsic cell frequency 15±2Hz).

Figure 6. Synchrony as a function of global re-wiring fraction and Type II fraction. (a) Synchrony of a mixed network of 50% Type I and 50% Type II neurons as a function of global re-wiring fraction P for no variance and uniform, Poisson and exponential distributions for both Type I HRW (light gray curves) and Type II HRW (black curves) scenarios. (b) Synchrony for a mixed network of Type I and Type II neurons, for different fractions of Type II neurons, where 0% Type II is a homogeneous Type I network and 100% is a homogeneous Type II network (P=0.15). (a,b) Insets show the differences between synchrony index values for Type II HRW and Type I HRW scenarios in the different re-wiring distributions (solid line: uniform ; dashed line: exponential, dotted line: Poisson). In all these simulations the intrinsic cell frequency was 15±2Hz, with synaptic weight W=0.01 mS/cm^2.

Figure 7. Synchrony as a function of heterogeneity in intrinsic neuron firing frequencies. (a) Synchrony of a mixed network of 50% Type I and 50% Type II neurons as a function of the percent spread around a mean neuronal firing frequency of 15 Hz for no variance and uniform, Poisson and exponential re-wiring distributions for Type I HRW (light gray curves) and Type II HRW (black curves) scenarios. These networks had a global rewiring fraction of P=0.15 and synaptic weights of 0.01 mS/cm^2. Inset shows the difference between synchrony index values of Type I and Type II HRW scenarios (solid line: uniform distribution; dashed line: exponential, and dotted line for Poisson). (b) Raster plots for Type I HRW (top row) and Type II HRW (bottom row) scenarios for exponential (left column) and Poisson (right column) re-wiring distributions with a 40% frequency spread.

Figure 8. Synchrony in networks with high connectivity clusters. a) Synchronization of mixed networks of 50% Type I and 50% Type II cells with P=0.15, and W=0.005 mS/cm^2. Here we interconnected a fraction of the most highly re-wired or least re-wired neurons to form connected clusters in the Poisson (top panel), uniform (middle panel) and exponential (bottom panel) distributions for the Type I HRW and Type II HRW cases. b) Example raster plots for exponential distribution networks in the Type I HRW (left column) and Type II HRW (right column) scenarios before the cluster is formed (top row), with a cluster consisting of the top 12% of highly re-wired neurons (middle row), and with a cluster consisting of the lowest 12% of re-wired neurons (bottom row) (panel numbers I-VI correspond to labeled points on curves in bottom panel of a).

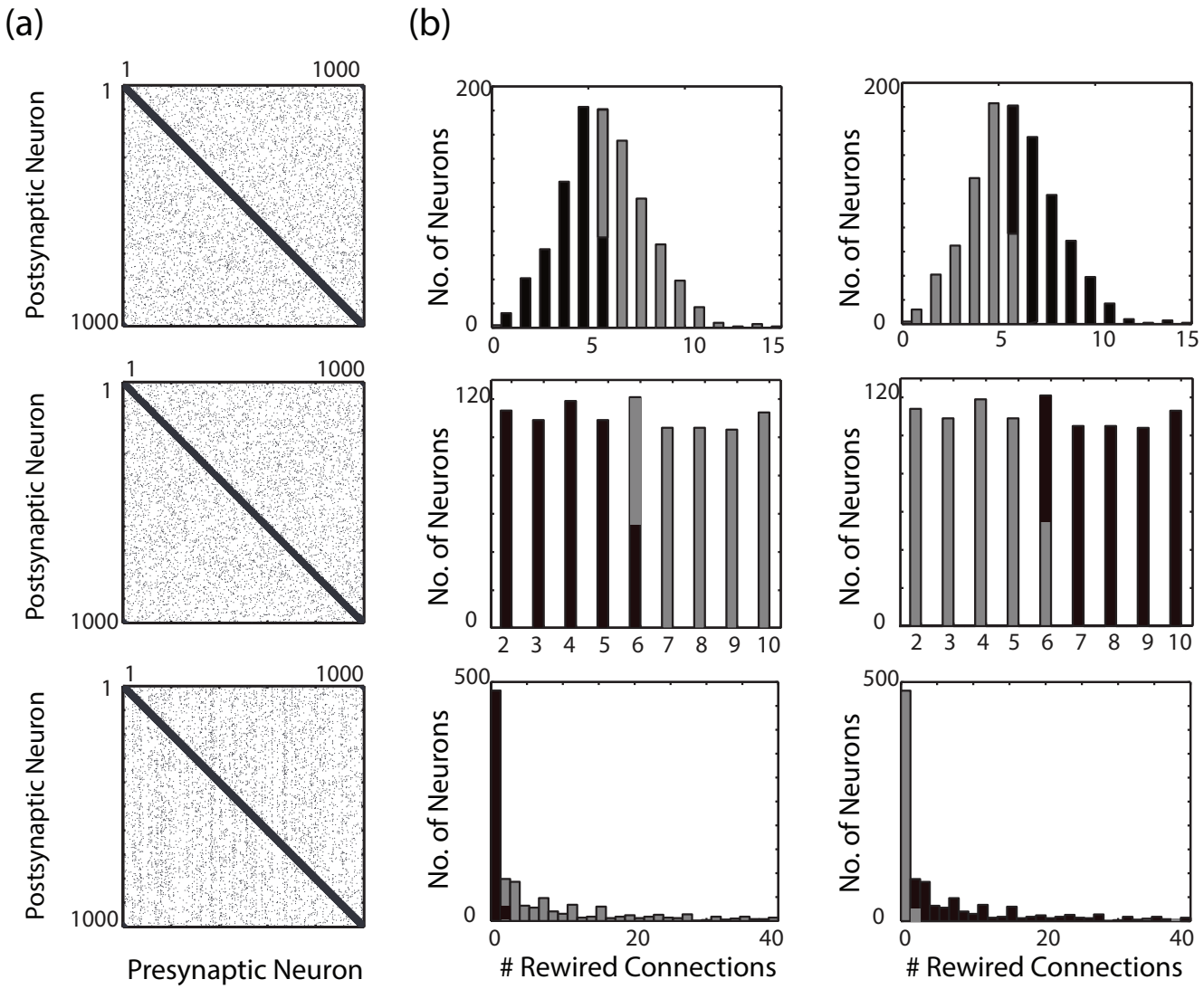

Figure 1 EN11275 29SEP2016

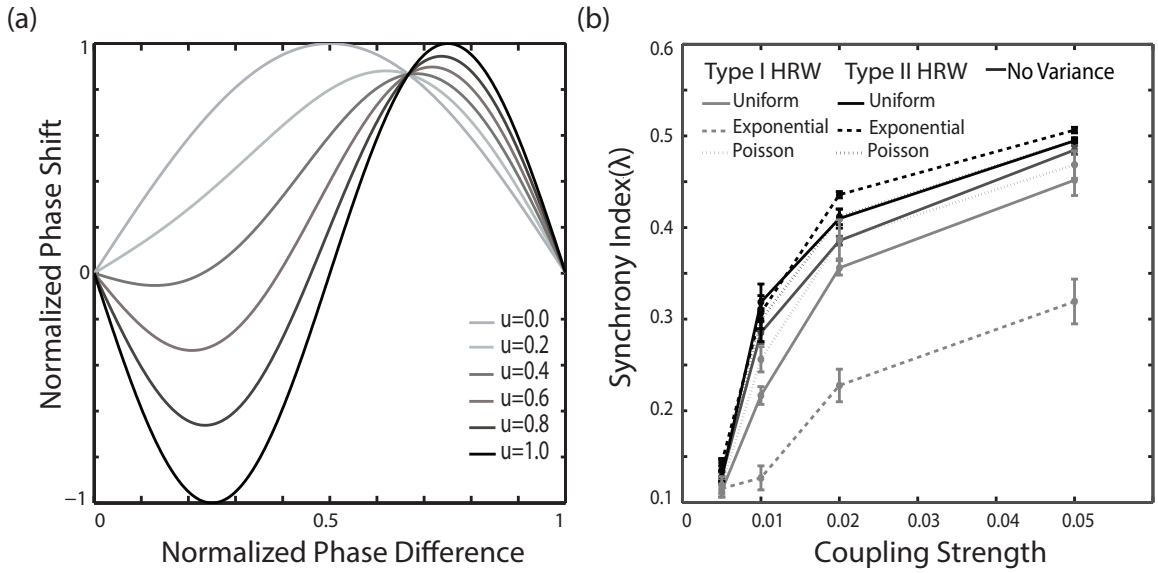

Figure 2 EN11275 29SEP2016

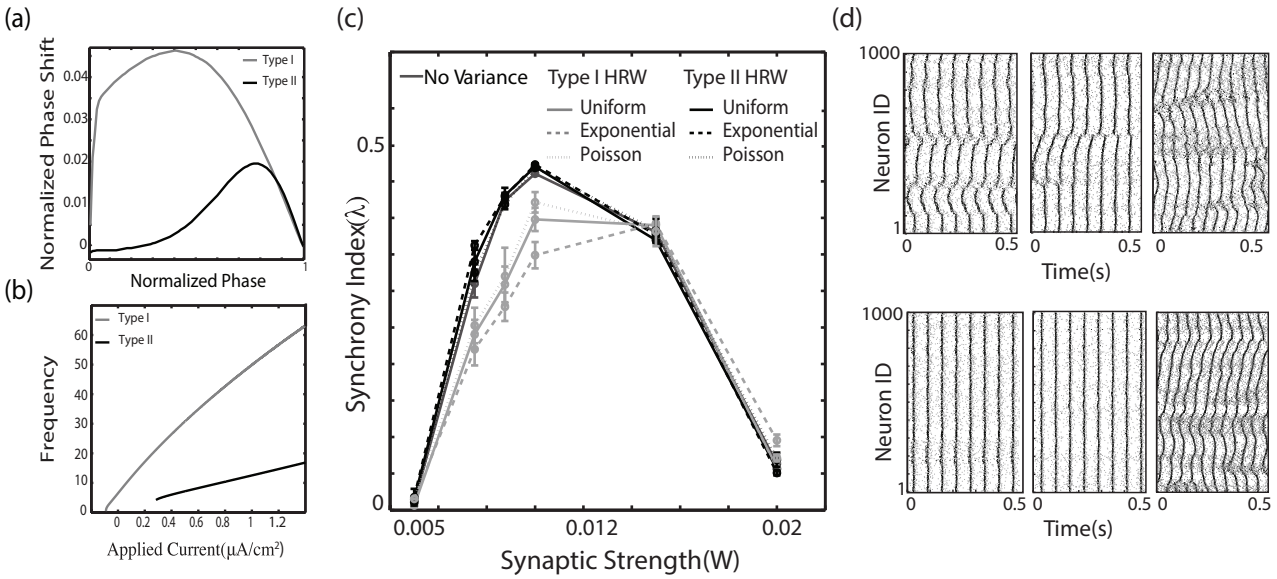

Figure 3 EN11275 29SEP2016

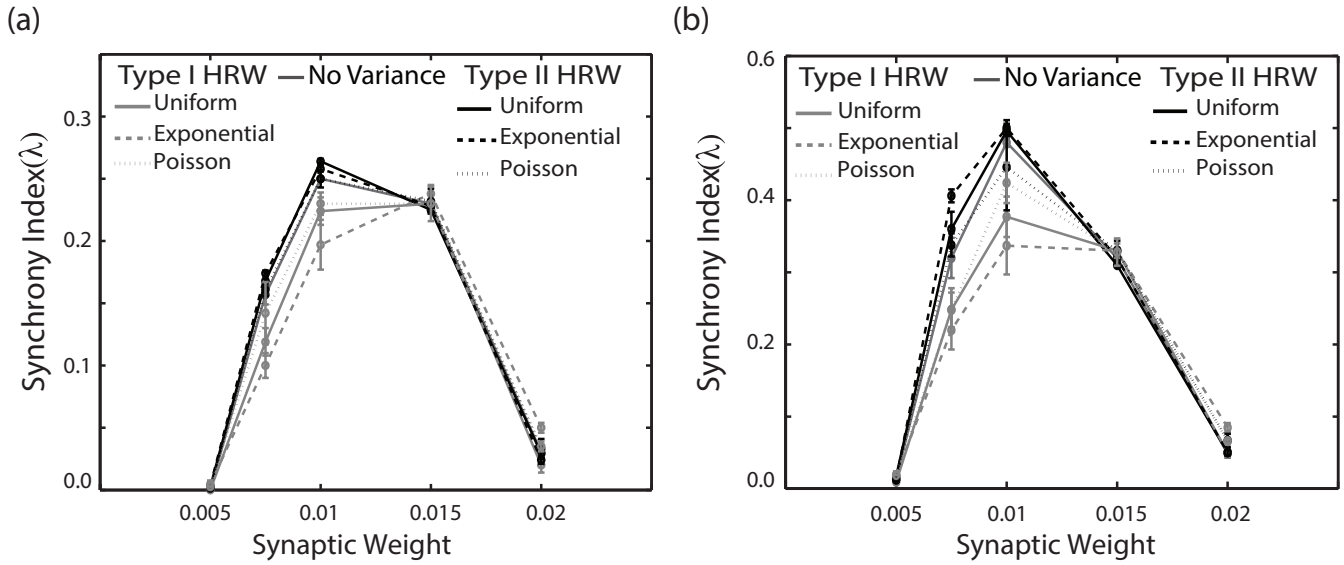

Figure 4 EN11275 29SEP2016

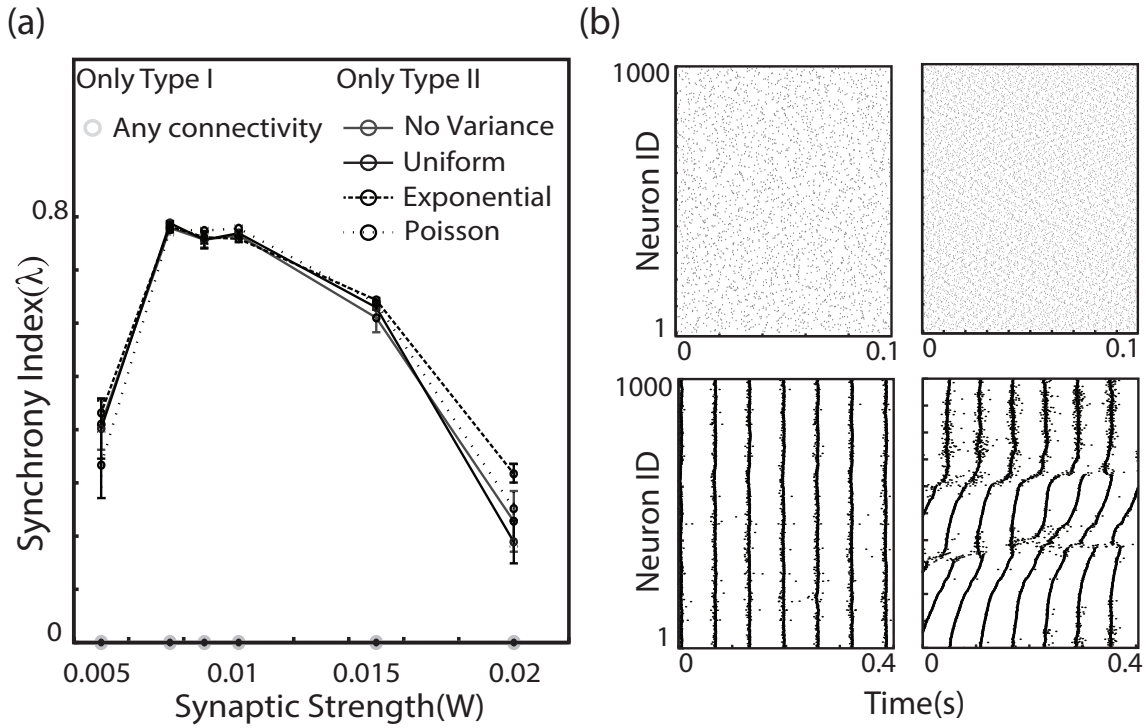

Figure 5 EN11275 29SEP2016

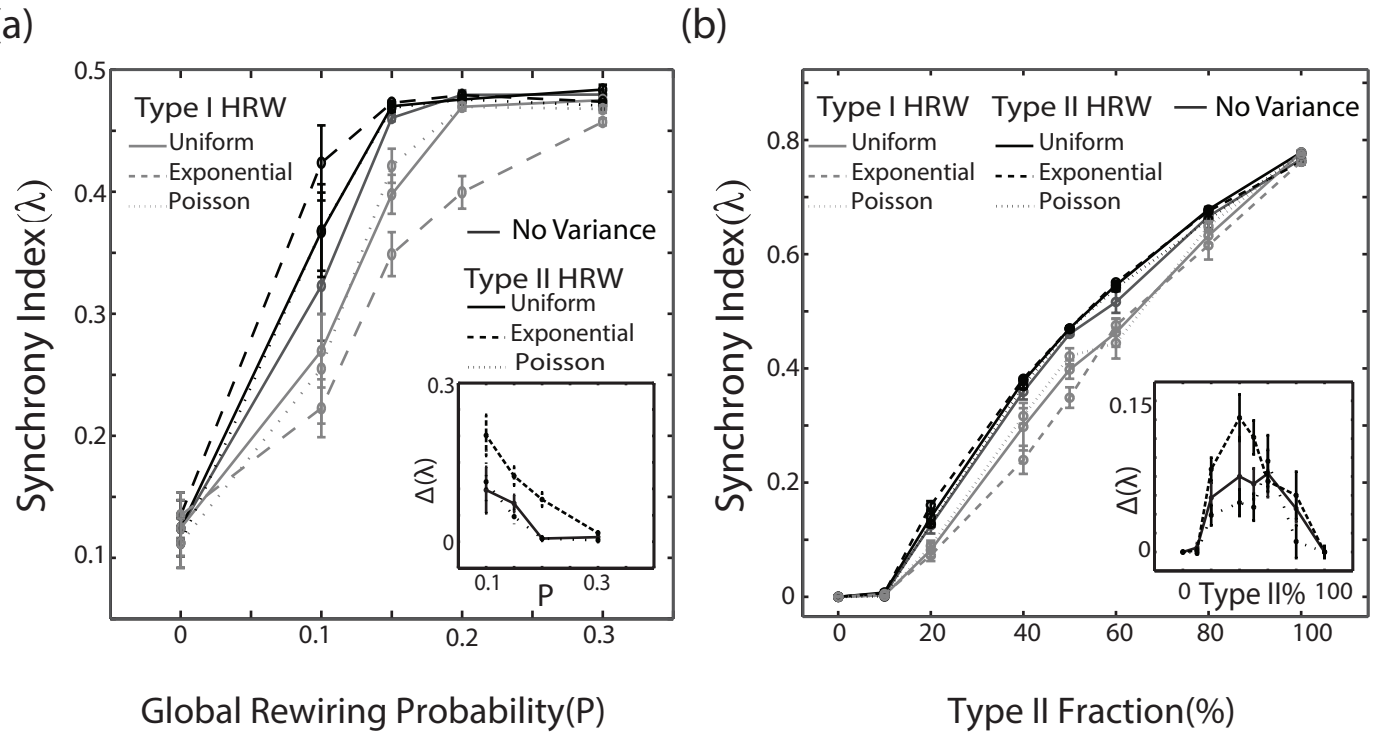

Figure 6 EN11275 29SEP2016

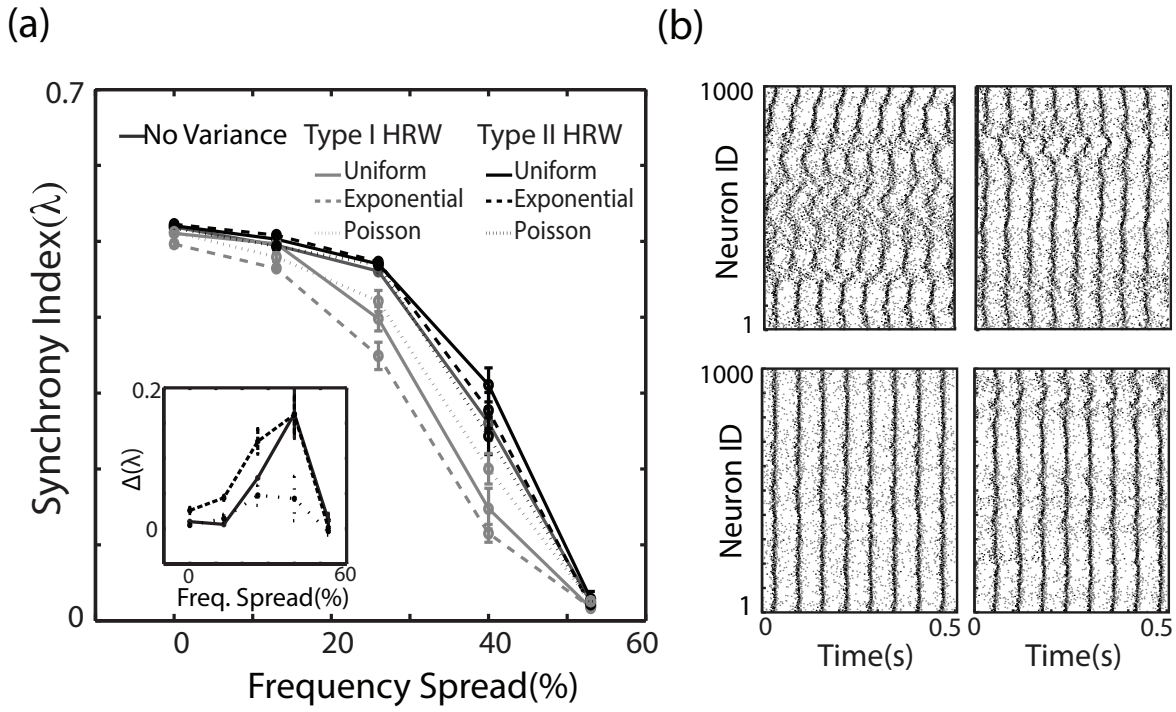

Figure 7 EN11275 29SEP2016

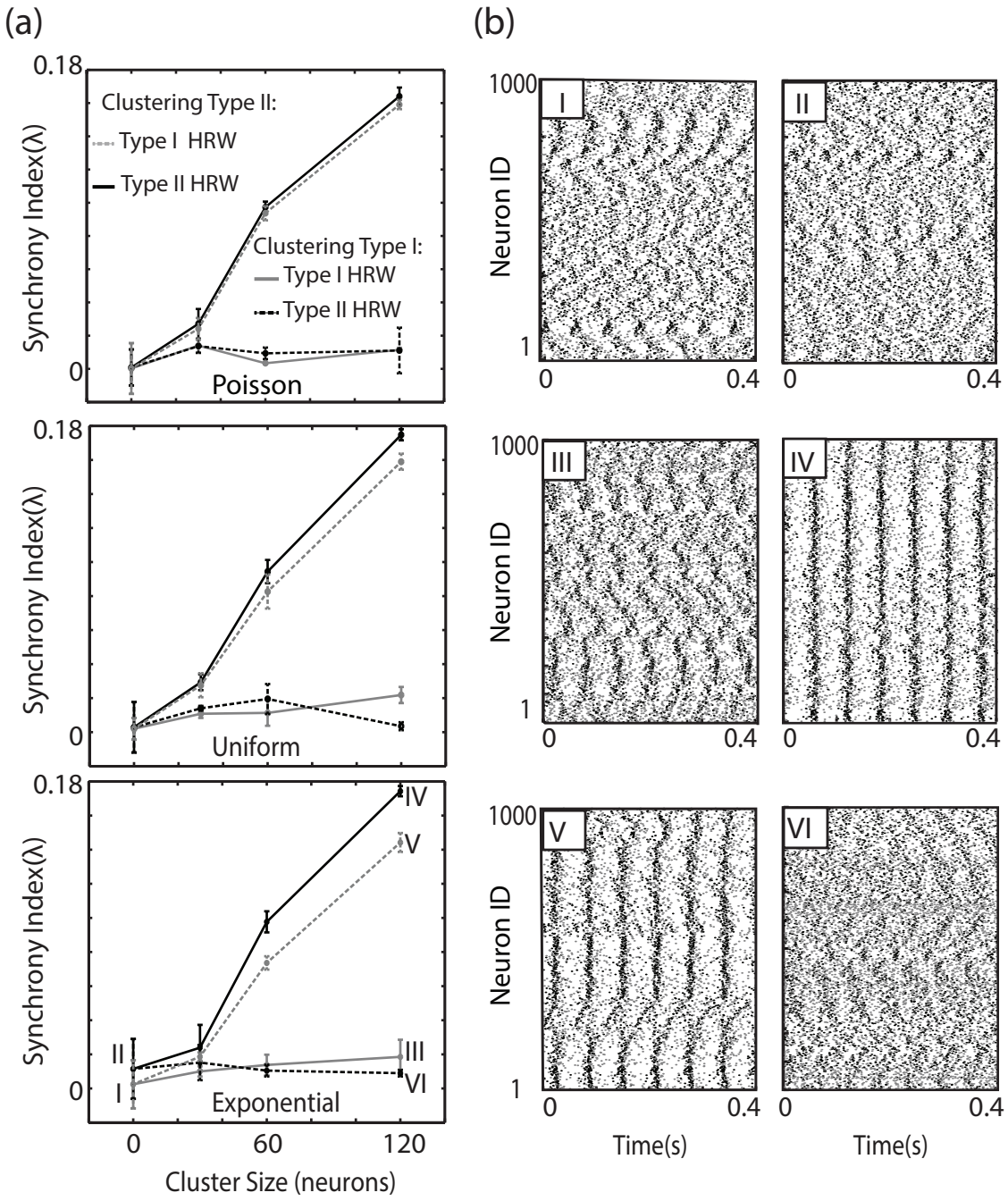

Figure 8 EN11275 29SEP2016